

Depolarization and Faraday effects in AGN Jets

E. Yushkov^{1,2}, I. N. Pashchenko³, D. Sokoloff^{1,4} and G. Chumarin¹

¹Department of Physics, Moscow State University, Leninskie Gory 1, 119991 Moscow, Russia

²Space Research Institute of the Russian Academy of Sciences (IKI), Profsoyuznaya st, 84/32 Moscow, Russia

³Lebedev Physical Institute of the Russian Academy of Sciences, Leninsky Prospekt 53, 119991 Moscow, Russia

⁴IZMIRAN, Kaluzhskoe Shosse 4, Troitsk, 108840 Moscow, Russia

Accepted 2024 October 29. Received 2024 October 17; in original form 2024 March 6

ABSTRACT

Radio interferometric observations of active galactic nuclei (AGN) jets reveal the significant linear polarization of their synchrotron radiation that changes with frequency due to the Faraday rotation. It is generally assumed that such depolarization could be a powerful tool for studying the magnetized plasma in the vicinity of the jet. However, depolarization could also occur within the jet if the emitting and rotating plasma are cospatial (i.e. the internal Faraday rotation). Burn obtained very simple dependence of the polarization on the wavelength squared for the discrete source and resolved slab that is widely used for interpreting the depolarization of AGN jets. However, it ignores the influence of the non-uniform large-scale magnetic field of the jet on the depolarization. Under the simple assumptions about the possible jet magnetic field structures, we obtain the corresponding generalizations of Burn’s relation widely used for galaxies analysis. We show that the frequency dependences of the Faraday rotation measure and polarization angle in some cases allow to estimate the structures of the jets magnetic fields.

Key words: galaxies: active – galaxies: jets – radiation mechanisms: non-thermal.

1 INTRODUCTION

Large-scale magnetic fields are thought to play a crucial role in launching, acceleration, and collimation of jets in active galactic nuclei (Meier, Koide & Uchida 2001; McKinney 2006; Komissarov et al. 2007; Blandford, Meier & Readhead 2019). Observationally, the most detailed information about the magnetic fields in active galactic nuclei (AGN) jets comes from polarimetric very long baseline interferometry (VLBI) experiments (e.g. Gabuzda 2018b). The radiation of parsec-scale AGN jets in the radio band, which is a synchrotron radiation of the ultra relativistic electrons in the jet magnetic field, is significantly linearly polarized (Pushkarev et al. 2023). The behaviour of synchrotron radiation, passing through the magnetically active media, which changes its linear polarization in a frequency-dependent manner (i.e. Faraday effect), opens up an indirect possibility of reconstructing magnetic fields based on the study of such depolarization.

While the ultra relativistic electrons are capable for the emission of the synchrotron radiation, the Faraday effects are mainly driven by the thermal magnetized plasma or, in general, the low-energy electrons (Jones & O’Dell 1977). These two populations of particles could be cospatial, producing the internal depolarization (Burn 1966). However, the relative importance of the external and internal Faraday effects is still not clear.

The observed polarization patterns of AGN jets suggest the presence of the large-scale helical magnetic field, see Gabuzda (2018a) for a review. Multifrequency polarimetric observations reveal the large-scale magnetic field component also in and around

the jets on kpc and pc scales (Perley, Bridle & Willis 1984; Asada et al. 2002; Gómez et al. 2011; Gabuzda, Knuettel & Bonafede 2015; Anderson, Gaensler & Feain 2016; Motter & Gabuzda 2016; Gabuzda et al. 2017; Knuettel, Gabuzda & O’Sullivan 2017; Pasetto et al. 2021) by the transverse gradients of the Faraday rotation measure, RM. Both observational data (Lisakov et al. 2021) and general relativistic magnetohydrodynamic (GRMHD) simulations (Broderick & McKinney 2010) suggest that such gradients are due to the magnetized sheath around the radiating jet plasma, while there is the evidence that the observed transverse gradients could trace the inner structure of the magnetic field (e.g. in ‘magnetic tower’ model, Mahmud, Gabuzda & Bezrukova 2009; Mahmud et al. 2013; Christodoulou et al. 2016; Gabuzda 2017; Gabuzda, Nagle & Roche 2018). Moreover, ‘inverse’ or ‘anomalous’ depolarization observed in some sources (Hovatta et al. 2012) with transverse RM gradient could imply the internal Faraday rotation in a helical magnetic field (Sokoloff et al. 1998; Homan 2012). The most mass multifrequency polarization VLBI observations of 191 sources from MOJAVE¹ sample at 8, 12, and 15 GHz (Hovatta et al. 2012) revealed the depolarization patterns that suggests the external Faraday screen, while some sources require the internal rotation. Detailed 10-frequency (from 1.4 to 15.4 GHz) polarimetric VLBI observations of 20 AGN jets (Kravchenko, Kovalev & Sokolovsky 2017) are consistent with this result. Broad-band (112 subbands over 14 GHz frequency range from 4 to 18 GHz) full-polarization JVLA observations of M87 radio jet which employed the QU-fitting method revealed the internal Faraday rotation in a helical magnetic field of the jet (Pasetto et al.

* E-mail: in4pashchenko@gmail.com (INP); sokoloff.dd@gmail.com (DS)

2021), that is consistent with earlier studies (Chen, Zhao & Shen 2011).

The multifrequency polarization data is usually interpreted using various relations between the magnetic field and polarization (e.g. Burn 1966; Tribble 1991; Sokoloff et al. 1998; Rossetti et al. 2008; Mantovani et al. 2009). When simultaneous broad-band multichannel data is available RM synthesis (Brentjens & de Bruyn 2005) and QU-fitting (Farnsworth, Rudnick & Brown 2011; O’Sullivan et al. 2012) techniques could be employed to, correspondingly, obtain the polarization signal and fit it with a simple analytical models (see Pasetto 2021 for a review). While they are shown to be capable to explore the magnetic field in kp-scale jet of M87 (Pasetto et al. 2021), spectrally resolve the polarized components of the unresolved radio sources (Pasetto et al. 2018) or to select a jet with a possible transverse RM gradients (Anderson et al. 2016), such dense frequency coverage is not attainable with modern VLBI. Thus, multifrequency VLBI polarization data of parsec-scale AGN jets is analysed using simple depolarization relations (Hovatta et al. 2012; Kravchenko et al. 2017) and, when the jet is transversely resolved, the qualitative large-scale magnetic field models are employed (Asada et al. 2002, e.g. the toroidal magnetic field to explain the transverse RM gradients).

One of the quite simple, productive, and correspondingly most frequently used depolarization relation obtained by Burn (1966) in context of discrete sources was later adopted by Sokoloff et al. (1998) for the discs of the spiral galaxies. Burn’s relation is successfully exploited for interpreting the AGN jets internal depolarization (e.g. Hovatta et al. 2012; Kravchenko et al. 2017; Park et al. 2019; Pasetto et al. 2021; Zobnina et al. 2023). However, the geometry of the jets and their expected magnetic configuration are obviously something different from the galactic discs. Of course, one can hope that the differences between discs and jets are not crucial enough to obtain the reasonable estimate of the magnetic field strength, bearing in mind that Sokoloff et al. (1998) provides the examples of the magnetic configurations where the conventional relations lead to the erroneous conclusions. A validation of that approach comes in particular from the fact that Burn (1966) and Sokoloff et al. (1998) departing from different points (discrete sources and discs) arrives to the same scaling. So it looks reasonable to analyse at some point the difference between disc and jets in context of the depolarization studies. This is just the aim of this paper. To be specific, we consider the depolarization by the large-scale jet magnetic field and intrinsic Faraday rotation from jet-like cylindrical objects with axial symmetry.

2 BURN’S RELATION

As we mentioned in the introduction the physical phenomenon underlying Burn’s formula is the Faraday rotation, which occurs due to the incoming phase difference between the right and left polarized waves (Ginzburg & Syrovatskii 1966). The difference between the refractive indices for these two waves is so small, that the main role here is played by the large distance, over which a rotation of the polarization plane occurs. Therefore the local polarization angle $\psi(r)$ can be determined, see, e.g. Sokoloff et al. (1998), by the integral expression along the line of sight:

$$\psi(r) = \psi_0(r) + R(r)\lambda^2, \quad \text{where} \quad R(r) = -K \int_{r_0}^r n \mathbf{B} dr. \quad (1)$$

The function $\psi_0(r)$ here represents the intrinsic position of the electric vector of the synchrotron emission, which is assumed to be perpendicular to the transverse component of the magnetic field \mathbf{B} , λ is the radiation wavelength, r_0 and r are the start and end points of

the beam passing through the active region, n is the number density of the thermal electrons and the notation K is used for the ratio $e^3/2\pi m^2 c^4$ (in cgs electromagnetic units), where c , e , and m are the speed of light, the electron charge, and mass correspondingly.

To calculate the depolarization effect from the extended astrophysical objects, e.g. galaxies and jets, it must be taken into account that each element along the line of sight can have its own emissivity $\varepsilon(r)$ – the energy emitted towards the observer per unit time per unit volume. Thus, the complex linear polarization P should be defined by the integration along the line of sight:

$$\frac{P}{P_0} = \int_{r_0}^r \varepsilon(r) \exp(2i(\psi_0(r) + R(r)\lambda^2)) dr \left| \int_{r_0}^r \varepsilon(r) dr \right|^{-1}, \quad (2)$$

where, following Ginzburg & Syrovatskii (1966), we assume that the emissivity $\varepsilon(r)$ is determined only by the square of the perpendicular component of the magnetic field.² Moreover, here and below we consider only a completely resolved sources, keeping in mind, that finite resolution, e.g. for the Gaussian beams, discussed by Burn (1966) and Sokoloff et al. (1998), could significantly complicate the analysis (see also Cioffi & Jones 1980).

Strictly speaking Burn’s result itself provided the complex polarization (2) of the synchrotron radiation from a homogeneous plate, which can be used as the approximation of a galaxy disc with a constant thickness $L = 2l$ (though Burn did not apply his slab model to a disc galaxy at all). Using the coordinate system referenced to the homogeneous plate, where y -axis is directed perpendicular to the ‘galaxy’ plane and to the ‘galaxy’ internal magnetic field $\mathbf{B} = (0, 0, -B_z)$, we direct the line of sight (the direction opposite to the direction of the emission) at the angle θ to the z -axis, see the left panel of the Fig. 1. For a constant magnetic field B_z and constant number density n from the equation (1) it is easy to calculate the function $R(y)$, substituting the variable r along the line of sight with the y coordinate along the y -axis and considering $dr = (0, dy, dy \operatorname{ctg}\theta)$:

$$R(y) = Kn \int_{-l}^y B_z \operatorname{ctg}\theta dy = Kn B_z \operatorname{ctg}\theta (l + y). \quad (3)$$

Then, introducing the so called intrinsic Faraday rotation measure $\mathcal{R} = 2KnB_z \operatorname{ctg}\theta l$, see e.g. Sokoloff et al. (1998), from the equation (2) it is possible to obtain Burn’s relation for the complex relative polarization P/P_0 , more conveniently for its absolute value – the polarization degree Π and its argument – the polarization angle Ψ :

$$\frac{P}{P_0} = \Pi \exp(2i\Psi) = \frac{\sin(\mathcal{R}\lambda^2)}{\mathcal{R}\lambda^2} \exp(2i(\psi_0 + \mathcal{R}\lambda^2/2)),$$

and $\Pi = \frac{\sin(\mathcal{R}\lambda^2)}{\mathcal{R}\lambda^2}, \quad \text{where} \quad \Psi = \psi_0 + \mathcal{R}\lambda^2/2.$ (4)

Thus, according to Burn’s formula, the polarization degree Π depends on the wavelength squared λ^2 as a sinc function, and the polarization angle Ψ – as a linear function with the slope coefficient $\text{RM} = \mathcal{R}/2$, usually called the Faraday rotation measure. However, it is important to understand that the observed polarization angle Ψ_{obs} follows the linear law except for discontinuities at $\mathcal{R}\lambda^2 = n\pi$, where sinc changes its sign. At these points the sign of the polarization degree Π , which is non-negative, does not change, but there is a jump of the exponent argument by $i\pi$. This jump corresponds to the

²This assumes that the spectral index of the radiation $\alpha = -1$, where the intensity depends on the frequency ν as ν^α . Thus, the intrinsic degree of polarization P_0 is 0.75.

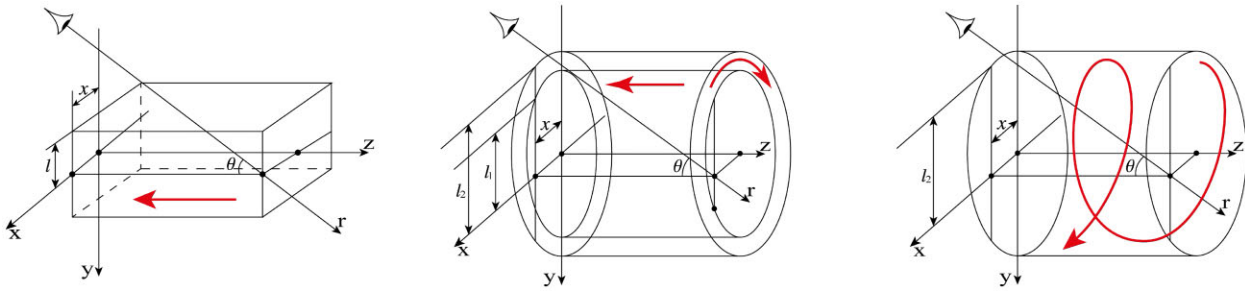


Figure 1. Schematic representation of the planar galaxy model (left panel), the two-zone jet model (middle panel), and the helical jet model (right panel). In all three cases the line of sight passed parallel to the coordinate Oxy-plane at an aiming distance x from it. In the two-zone jet model l_1 and l_2 are the projections of the inner radius ρ_1 and the outer radius ρ_2 on the y -axis. The model magnetic fields \mathbf{B} are schematically indicated by bold red lines. Detailed descriptions of each model are presented in the Sections 2, 3, and 4.

change of the polarization angle by $\pi/2$ and, as a result, the linear dependence transforms into the well-known sawtooth dependence with amplitude $\pi/2$. Such type of the sawtooth structure also occurs in a more complex field models with the complex polarization having one or more zeros – in particular, for jet magnetic field models discussed below.

Finally, note that the simple form of Burn’s results (4) follows from a number of assumptions that are reasonable only as an initial approximation. One have to keep in mind that the real systems are significantly more complex. However, talking in this paper about AGN jets, we limit ourselves to the similar assumptions, so it makes sense to list them again. First of all, we assume the constant number density n and the emissivity $\varepsilon(r)$, determined only by the square of the perpendicular component of the magnetic field implying spectral index $\alpha = -1$ and $P_0 = 0.75$, by analogy with the reasoning of the classical work Ginzburg & Syrovatskii (1966). Second, Burn’s formula assumes a constant initial positional angle ψ_0 , as the angle between the observer’s chosen direction \mathbf{N} on the celestial sphere and the electric wave field, oscillated parallel to the vector product $\mathbf{B} \times d\mathbf{r}$. Then, the constant angle ψ_0 in (4) follows from the constant magnetic field in the galactic disc. We use the same assumption, ψ_0 is the angle between the vector \mathbf{N} and the vector $\mathbf{B} \times d\mathbf{r}$, for jets also. Finally, the linear dependence of the polarization angle Ψ on the wavelength squared λ^2 is a direct consequence of the magnetic field symmetry with respect to $y = 0$, see remarks in Appendix A. For jets we consider the azimuthally symmetric cases leading to similar conclusions. Under more complicated assumptions, this dependence can have much more complex character, see e.g. Sokoloff et al. (1998). The discussion of the assumptions correctness in the light of the observed data and the approximation of more complex AGN jet models are left by us for the future works.

3 TWO-ZONE MAGNETIC FIELD MODEL

The derivation of the relation similar to Burn’s formula for cylindrical structures is also possible. The main question here is how to setup such a structure in such a way that, first, the main features of the depolarization can be predicted and, secondly, the simplest and most convenient formula comparable to Burn’s relation can be obtained. As a zeroth order approximation consider a cylindrical model consisting of two zones: an inner cylinder ($0 \leq \rho \leq \rho_1$) and an outer cylindrical shell ($\rho_1 \leq \rho \leq \rho_2$), where as in the traditional cylindrical coordinate system ρ is the Euclidean distance from the z -axis and φ is the azimuthal angle between the x -axis and the point projection on the Oxy-plane. Assume that in the central part the constant longitudinal magnetic field $\mathbf{B} = (0, 0, -B_z)$ is directed

along the z -axis, and at the periphery the azimuthal field is defined as $\mathbf{B} = (B_\varphi \sin \varphi, -B_\varphi \cos \varphi, 0)$, see the middle panel of Fig. 1. Note that such structure could be considered as an approximation of the force-free magnetic field, where the pitch-angle of the field increases with distance from the jet axis (Lyutikov, Pariev & Gabuzda 2005; Clausen-Brown, Lyutikov & Kharb 2011) or magnetohydrodynamic jet model with the ‘core’ of the longitudinal magnetic field (Beskin, Kniazev & Chatterjee 2023).

Assume that the line of sight is directed exactly to the centre of the jet at an angle θ to the z -axis, then the case with $\theta = 90^\circ$ can reasonably be called degenerate, since there is no magnetic field component directed along the line of sight. For $\theta \neq 90^\circ$ the peripheral region provides only the intensity of the radiation, while the rotation of the polarization plane is performed by the central region, similar to Burn’s formula (4). In this case, as shown in Appendix B, the polarization degree and the polarization angle will be equal to

$$\Pi = \frac{1}{1 + \gamma} \frac{\sin(\mathcal{R}_1 \lambda^2)}{\mathcal{R}_1 \lambda^2} - \frac{\gamma}{1 + \gamma} \cos(\mathcal{R}_1 \lambda^2) \quad \text{and} \quad \Psi = \mathcal{R}_1 \lambda^2 / 2, \quad (5)$$

where $\mathcal{R}_1 = 2KnB_z \operatorname{ctg} \theta \rho_1$ is the intrinsic Faraday measure and $\gamma = \varepsilon_2(\rho_2 - \rho_1)/\varepsilon_1 \rho_1$ characterizes the ratio of intensities at the periphery and in the centre. As discussed in the Section 2, we assumed that the emissivities are determined only by the square of the perpendicular component of the magnetic field, in other words $\varepsilon_1 = \kappa B_z^2 \sin^2 \theta$ and $\varepsilon_2 = \kappa B_\varphi^2$, where κ is the proportionality factor.

It is interesting that even within such a simple consideration, the difference between the radiation from a flat galaxy (4) and from an AGN jet (5) is evident. For example, for small $\mathcal{R}_1 \lambda^2$, when θ is close to 90° or λ is close to 0, the synchrotron radiation is initially depolarized: $\Pi(0) = |1 - \gamma|/|1 + \gamma| \leq 1$. The reason for this is that in the central and peripheral regions the electric fields oscillate along the different directions: the electric field is perpendicular to the x -axis at the periphery and parallel to the x -axis at the centre. Thus, the modulus of $\Pi(\lambda^2)$, which for Burn’s formula has the form of a sinc, is now the difference between the sinc and the cosine function, where the mutual contribution of the components is determined by γ . This can be seen in Fig. 2, where the dependences of the polarization degree Π on the wavelength λ for different angles, θ , and aiming distances, x , are shown. The low value of polarization, called below the polarization drop, is clearly seen for the jet centre lines – blue lines with $x = 0.05\rho_2$ – for all three cases: $\theta = 90^\circ$ (top panel), $\theta = 85^\circ$ (middle panel), and $\theta = 45^\circ$ (bottom panel). Another example is the dependence of the polarization angle Ψ on the wavelength squared λ^2 . For Burn’s relation, this dependence is

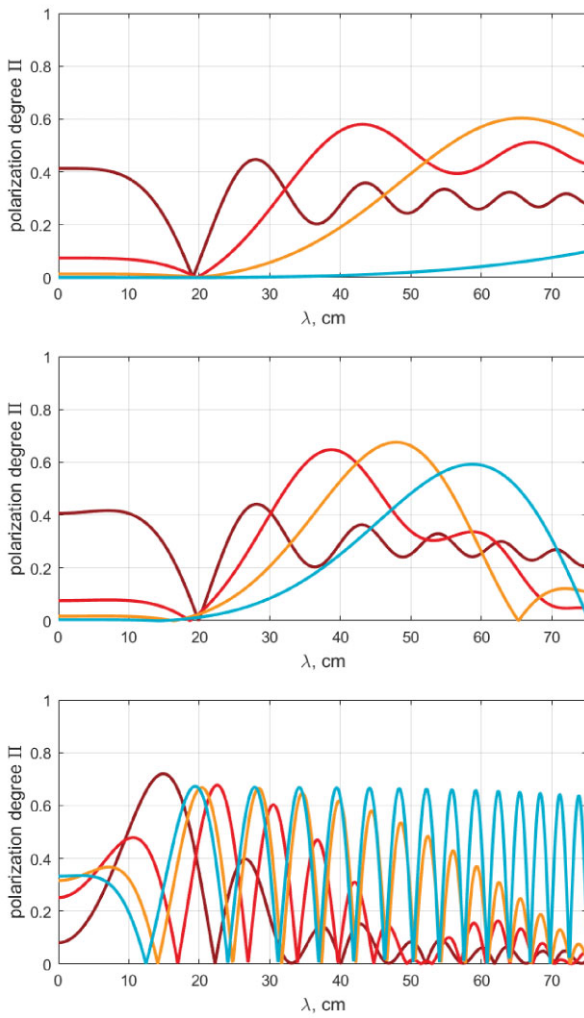


Figure 2. Two-zone magnetic field model. Dependences of the polarization degree Π on wavelength λ for three angles: $\theta = 90^\circ$ (top panel), $\theta = 85^\circ$ (middle panel), and $\theta = 45^\circ$ (bottom panel). The colours of the lines correspond to different aiming distances: $x = 0.05\rho_2$ (blue), $x = 0.25\rho_2$ (orange), $x = 0.50\rho_2$ (red), and $x = 0.75\rho_2$ (brown). The azimuthal and longitudinal magnetic fields here are $KnB_\varphi = 0.01$ and $KnB_z = 0.005$, so the Faraday rotation measure varies from 0 to about 50 rad m^{-2} for $\theta = 90^\circ$, see the equation (8) and Fig. 5.

linear (4) with the polarization angle $\Psi = \psi_0$ for small λ . Finding this ψ_0 is an important observational problem, which is feasible but requires multiple measurements at different wavelengths. For the jet the angle Ψ has no ψ_0 because of the parity of the magnetic field component along the line of sight, see Appendix A. It would be more correct to say that in order for the angle $\Psi = 0$ at small λ , it is necessary to count the polarization position angle from the direction perpendicular to the axis of the jet in the plane of the sky, x -axis. Note also that the actual observed polarization angle Ψ_{obs} dependence is not a linear, but sawtooth with discontinuities of 90° , where formula (5) for Π changes sign.³ Especially interesting is the situation at small wavelengths, when the $\pi/2$ jump can also be at $\lambda = 0$. For example, in the case when formula (5) gives a negative value for

³The example which shows the typical sawtooth dependence of $\Psi(\lambda^2)$ for helical magnetic field Section 4 is shown in Fig. 4. For two-zone model, the dependence is similar.

$(1 - \gamma)/(1 + \gamma)$. In other words, at small wavelengths the observed polarization angle $\Psi_{\text{obs}} = 0$, if $\gamma < 1$, and $\Psi_{\text{obs}} = \pi/2$, if $\gamma > 1$.

Now consider the line of sight that does not pass through the centre, but is parallel to the Oyz-plane at a distance of x from the axis of the jet. Suppose that this aiming distance x is small enough that the line still passes through two zones: the central one with a field B_z parallel to the jet axis and the peripheral one with a constant azimuthal field B_φ . Let's neglect the change of the azimuthal field rotation along line of sight in the outer cylindrical ring, i.e. assume that the angle between the magnetic field and the line at periphery does not change and is equal to φ_0 : $\cos \varphi_0 = x/\rho_2$. Calculations similar to those made in the Section 2, see Appendix B, allow us to calculate the complex polarization P/P_0 . Since the magnetic field $\mathbf{B}(y)$ along the line of sight turns out to be an even function with respect to $y = 0$, and the initial position angle $\psi_0(y)$ on the contrary is an odd function (due to the rotation of the azimuthal magnetic field), the polarization angle Ψ again turns out to be a linear function of the wavelength squared, see Appendix A:

$$\Psi = (\mathcal{R}_2 + \mathcal{R}_1/2)\lambda^2. \quad (6)$$

The slope of this linear dependence is determined by the difference of two intrinsic Faraday measures corresponding to the central and peripheral parts:

$$\mathcal{R}_1 = 2KnB_z \operatorname{ctg} \theta l_1 \quad \text{and} \quad \mathcal{R}_2 = KnB_\varphi x(l_2 - l_1)/\rho_2, \quad (7)$$

where $l_1 = (\rho_1^2 - x^2)^{1/2}$ and $l_2 = (\rho_2^2 - x^2)^{1/2}$. It is clearly seen that the Faraday rotation measure $\text{RM} = \mathcal{R}_2 + \mathcal{R}_1/2$ changes with both the angle θ and the aiming distance x (see e.g. the middle panel of Fig. 5). This implies that it is possible to reconstruct the internal structure of the jet magnetic field by measuring this slope for different x . Such an inverse problem is interesting in itself, but we leave it for the next paper and limit ourselves to noting that it can be done in principle.

Similarly, as shown in Appendix B, the expression for the degree of polarization Π can be obtained:

$$\Pi = \frac{1}{1 + \gamma} \frac{\sin(\mathcal{R}_1\lambda^2)}{\mathcal{R}_1\lambda^2} + \frac{\gamma}{1 + \gamma} \frac{\sin(\mathcal{R}_2\lambda^2)}{\mathcal{R}_2\lambda^2} \cos((\mathcal{R}_2 + \mathcal{R}_1)\lambda^2 + 2\psi_0),$$

$$\text{where } \gamma = \frac{\varepsilon_2(l_2 - l_1)}{\varepsilon_1 l_1} = \frac{B_\varphi^2 \rho_2^2 - x^2 \sin^2 \theta}{B_z^2 \rho_2^2 \sin^2 \theta} \frac{l_2 - l_1}{l_1} \quad (8)$$

It is seen that, as well as for the line of sight incident to the centre, the polarization degree is a superposition of the sine and cosine functions. Their ratio is determined by the relative emissivity γ of the central and peripheral regions. Besides, there is an additional term in cosine's argument ψ_0 : $\cos \psi_0 = x \cos \theta / \sqrt{\rho_2^2 - x^2 \sin^2 \theta}$, close to $\pi/2$ at small aiming distances x , which gives a difference of sine and cosine, and hence a reduced polarization degree $\Pi(0) = |1 - \gamma|/|1 + \gamma|$ at small values of λ .

Fig. 2 shows the results for the equation (8) for three angles θ at different panels, revealing a clear difference from Burn's relation (4) – the maximum value of the polarization degree does not correspond to small wavelengths. The degenerate case shown in the top panel has another difference mentioned earlier – the polarization may not tend to zero at long wavelengths, but to some constant level. However, already at angles close to $\pi/2$, e.g. the middle panel of Fig. 2, this situation is different and the polarization degree converges, albeit slowly, to zero with increasing λ . A similar situation is observed at small aiming distances, that corresponds to the blue lines in Fig. 2. As mentioned in Appendix B, it is possible that the polarization degree oscillates like a trigonometric function without decreasing. In the general case it can be stated that the observed polarization of jet radiation will be more difficult to analyse. First, because of the reduced degree: for a large class of parameters there are no values

of the polarization degree (2) close to unity. And second, because of the difficulty in predicting at which wavelengths the maximally polarized radiation will be observed.

4 HELICAL MAGNETIC FIELD MODEL

The two-zone model has highlighted the main differences between the polarization of radiation from galaxies and jets. Apart from the polarization drop at a short wavelengths and the direct proportionality between the polarization angle and the wavelength squared, the dependence of the polarization properties on the aiming distance x seems to be the most interesting. This is due to the axial symmetry of the jet and the fact that the aiming distance uniquely determines the region through which the radiation has passed. However, the two-zone model is inappropriate for a correct study of the aiming distance x dependence of the depolarization, since this model contains the separation boundary between the longitudinal field B_z and the azimuthal field B_φ . So it worth to consider another jet model – with a helical magnetic field.

Consider a cylinder of radius ρ_2 extended along the z -axis, see the right panel of Fig. 1, with the helical magnetic field B :

$$\mathbf{B} = (B_\varphi \sin \varphi(y), -B_\varphi \cos \varphi(y), -B_z), \quad (9)$$

where the angle $\varphi(y)$ now depends not only on the aiming distance x , but also on y -coordinate, as $\cos \varphi = x/(x^2 + y^2)^{1/2}$, where $y \in [-l_2, l_2]$ and $l_2 = (\rho_2^2 - x^2)^{1/2}$. Again, due to the axial symmetry, such a magnetic field along the line of sight is defined by the even function, so all the results of Appendix A are still applicable. Appendix C presents the example of the complex polarization calculation for a line of sight passing at the aiming distance x from the jet axis. Of course, the specific relations for the polarization angle and the degree of polarization depend on the radial profile of the magnetic field components. However due to the symmetry of the field, the polarization angle turns out to be proportional to the wavelength squared in all cases considered: $\Psi = RM\lambda^2$, see Fig. 4. In Appendix C, we describe three cases: (A) with a toroidal magnetic field component growing with distance to the jet axis $B_\varphi(\rho) = B_\varphi\rho/\rho_2$ and $B_z = \text{const}$, (B) with a constant magnetic field $B_\varphi = \text{const}$ and $B_z = \text{const}$, and (C) with the toroidal component decreasing with distance from the centre $B_\varphi(\rho) = B_\varphi\rho_2/\rho$ and $B_z = \text{const}$. For all three cases, the Faraday rotation measure can be computed explicitly:

$$\begin{aligned} (A): \quad & RM = KnB_\varphi xl_2/\rho_2 + KnB_z \operatorname{ctg}\theta l_2, \\ (B): \quad & RM = KnB_\varphi x \ln |(\rho_2 + l_2)/x| + KnB_z \operatorname{ctg}\theta l_2, \\ (C): \quad & RM = KnB_\varphi \rho_2 \operatorname{arctg}(l_2/x) + KnB_z \operatorname{ctg}\theta l_2, \end{aligned} \quad (10)$$

but it looks the simplest for the first case (A), which will be discussed further. The dependences of RM on the aiming distance x/ρ_2 are shown in Fig. 5. Note that the Faraday rotation measure can be represented as the sum of two intrinsic measures:

$$\frac{\Psi}{\lambda^2} = RM = \frac{\mathcal{R}}{2} = \mathcal{R}_2 + \frac{\mathcal{R}_1}{2} = KnB_\varphi \frac{xl_2}{\rho_2} + KnB_z \operatorname{ctg}\theta l_2, \quad (11)$$

which are determined by the longitudinal B_z and azimuthal B_φ field components. The first is an even x -function with respect to the jet centre and the second is an odd one, resulting in an asymmetric profile of the Faraday rotation measure with respect to $x = 0$. The profile of such an asymmetric dependence, case (A), for the angle $\theta = 45^\circ$ is shown in the top panel of Fig. 5 (solid line), as well as its symmetric (dotted line) and antisymmetric (dashed line) components. As the angle θ approaches 90° , the even component disappears, leaving only the odd component (dashed line). Thus,

the symmetric and asymmetric parts of the observationally obtained profiles allow us to estimate the relative strength of the longitudinal and azimuthal magnetic fields. The middle panel shows the Faraday rotation measure profiles for $\theta = 90^\circ$ and for different magnetic field distributions: the increasing field (case A, solid line), the constant field (case B, dashed line), and the decreasing field (case C, dotted line). Since the longitudinal magnetic field in these cases does not rotate the polarization plane, the profiles are odd with respect to $x = 0$, but at the same time they have a different structure. This implies that the distribution of the azimuthal magnetic field in jet-like structures can be reconstructed from the similar observed profiles. Note again that the discussed rotation measure RM determines the slope of the dependence $\Psi(\lambda^2)$. For example, the middle panel of Fig. 5 shows that RM, and hence the slope of the dependence, increases toward the edge of the jet, from the blue line ($x = 0.05$) to the brown line ($x = 0.75$). This is also seen in Fig. 4, where the slope increases from the blue to the brown line – but the dependence itself is not linear, but saw-toothed. As mentioned earlier, the jumps in the linear dependence occur at the wavelengths where the sign of Π changes. Thus, the sawtooth line oscillates in the band of 90° , but at different levels. These different levels are determined by the first sign change of Π . For example, Fig. 4 shows that for the red line ($x = 0.5$) the sign changes almost immediately, while for the blue line ($x = 0.05$) sign changes later than for the others.

The degree of polarization Π , see Appendix C, also depends on the magnetic field profiles. For the most calculationally convenient case (A), when the field grows from the centre of the jet, the degree of polarization can be written as

$$\Pi = \frac{1}{1 + \gamma} \left(1 + \sqrt{3\gamma} \frac{\partial}{\partial \xi} \right)^2 \frac{\sin \xi}{\xi}, \quad \text{where } \xi = \mathcal{R}\lambda^2, \quad (12)$$

and γ is a more complicated structure than simply the ratio of the squared field components:

$$\gamma = \frac{l_2^2 B_\varphi^2}{3\rho_2^2 (B_z \sin \theta - x B_\varphi \cos \theta / \rho_2)^2}. \quad (13)$$

Fig. 3 demonstrates the dependences of the polarization degree Π on the wavelength λ for three angles: $\theta = 90^\circ$ (top panel), $\theta = 85^\circ$ (middle panel), and $\theta = 45^\circ$ (bottom panel). The colours of the lines correspond to different aiming distances: $x = 0.05\rho_2$, $x = 0.25\rho_2$, $x = 0.50\rho_2$, and $x = 0.75\rho_2$, which are chosen to be the same as for the two-zone field model. The dependences generally look similar to those for the two-region model shown in Fig. 2. However, there are no cases of non-decreasing polarization degree at long wavelengths. This can be seen from the small difference between the upper and middle panels for the rays near the centre of the jet $x \approx 0$, the blue lines. There are also no oscillations with a constant amplitude, i.e. the degree of polarization decreases rapidly with increasing wavelength.

Finally, let's note another similarity between Figs 3 and 2 – the depression of the polarization degree at small wavelengths. Incidentally, to demonstrate the behaviour of the polarization degree at small wavelengths, we plot the dependences $\Pi(\lambda)$, rather than the more familiar dependences $\Pi(\lambda^2)$. In Appendix C, we obtain the following expression for the degree of polarization at short wavelengths $\Pi(0) = |1 - \gamma|/|1 + \gamma|$, where

$$\gamma = \int_0^{l_2} B_\varphi^2 \sin^2 \varphi(y) dy \left| \int_0^{l_2} (B_z \sin \theta - B_\varphi \cos \varphi(y) \cos \theta)^2 dy \right|^{-1}$$

Thus such polarization drop has an even profile with respect to the jet axis for $\theta = 90^\circ$, and odd for other angles, see the bottom panel of Fig. 5. Furthermore, in this panel we can clearly see that there are regions in the jet with $(1 - \gamma)/(1 + \gamma) < 0$ (near the centre) and $(1 -$

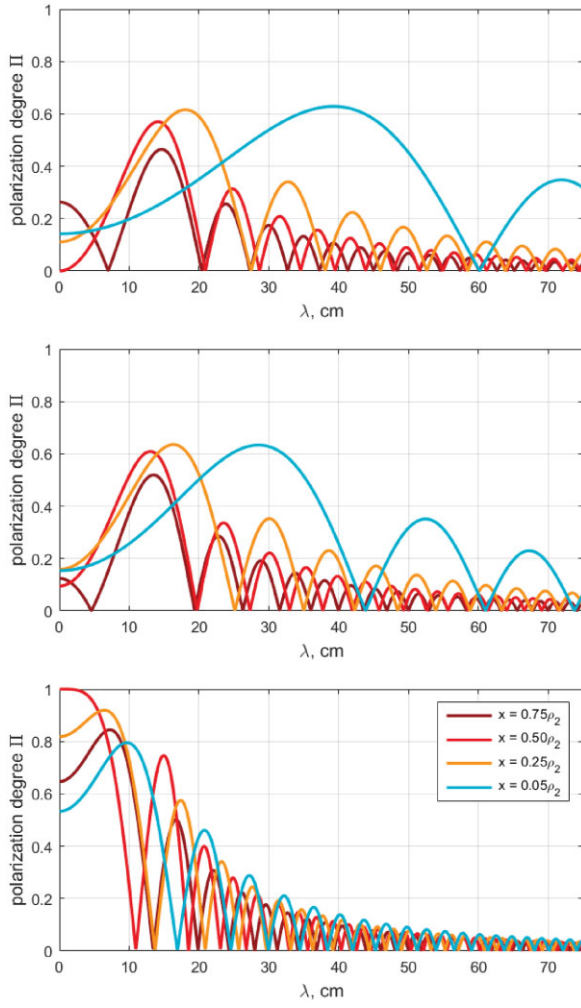


Figure 3. Helical magnetic field model. Dependences of the polarization degree Π on wavelength λ for three viewing angles: $\theta = 90^\circ$ (top panel), $\theta = 85^\circ$ (middle panel), and $\theta = 45^\circ$ (bottom panel). The colours of the lines correspond to different aiming distances: $x = 0.05\rho_2$ (blue), $x = 0.25\rho_2$ (orange), $x = 0.50\rho_2$ (red), and $x = 0.75\rho_2$ (brown). The azimuthal and longitudinal magnetic fields are $KnB_\varphi = 0.01$ and $KnB_z = 0.005$ that the internal Faraday measures vary from 0 up to about 50 rad m $^{-2}$ for $\theta = 90^\circ$, see the equation (12) and Fig. 5.

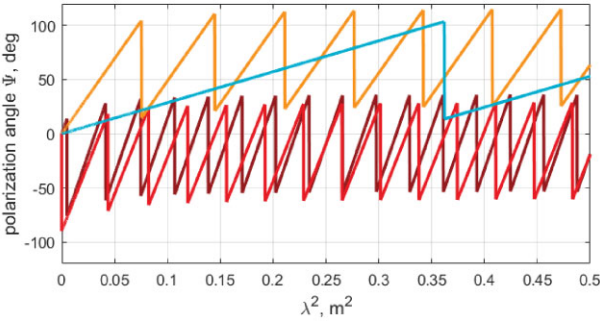


Figure 4. Typical dependence of the polarization angle Ψ on the square of the wavelength λ^2 for the helical magnetic fields model, $\theta = 90^\circ$. The polarization angle is counted from the x -axis shown in Fig. 1 and corresponding to the direction perpendicular to the projection of the jet axis on to the plane of the sky, see Appendix A. The parameters and colours here are the same as in the top panel of Fig. 3. The sawtooth form is associated with the sign change of the formula for the polarization degree Π .

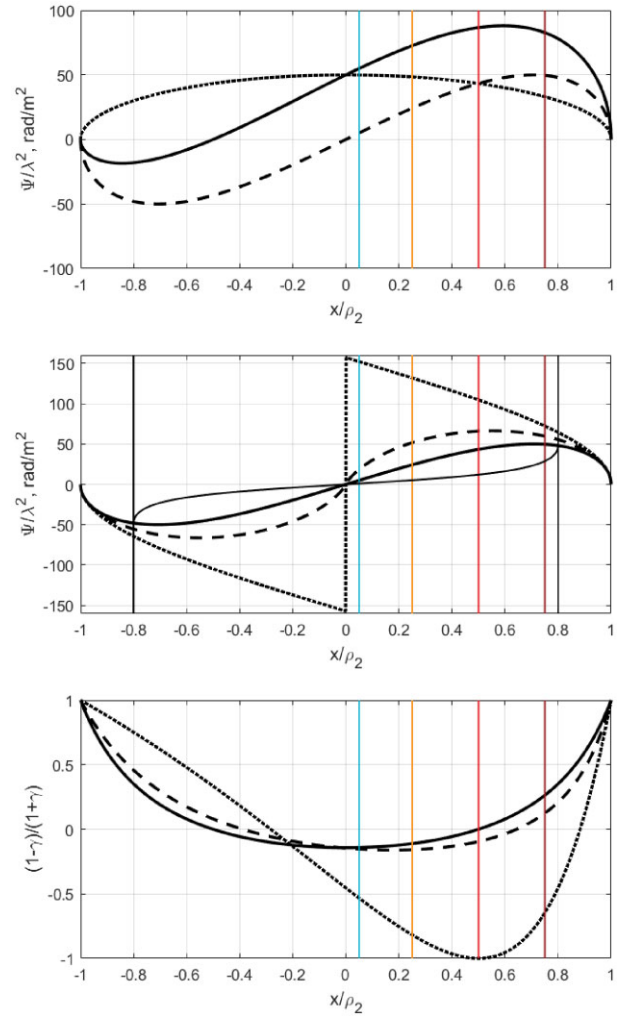


Figure 5. Top panel shows the dependences of the Faraday rotation measures Ψ/λ^2 on the aiming distance x/ρ_2 for the helical field at angle $\theta = 90^\circ$ (dashed line) and at angle $\theta = 45^\circ$ (solid line). At angle $\theta = 90^\circ$, the curve is odd relative to the jet axis. At angle $\theta = 45^\circ$ the curve is a superposition of the even component (dotted line) and the odd component (coincides with the dashed line). The middle panel shows the dependences of the Faraday rotation measures Ψ/λ^2 on the aiming distance x/ρ_2 for different magnetic fields: for the increasing field (solid line), for the constant field (dashed line), for the decreasing field (dotted line), and also for the two-zone model (thin solid line, for $-0.8 < x/\rho_2 < 0.8$). The bottom panel shows the dependences of the ratio $(1 - \gamma)/(1 + \gamma)$ on the aiming distance x/ρ_2 , the modulus of which determines the degree of polarization at small wavelengths for different angles: $\theta = 90^\circ$ (solid line), $\theta = 85^\circ$ (dashed line), and $\theta = 45^\circ$ (dotted line). The azimuthal and longitudinal magnetic fields are the same as in Figs 2 and 3, $KnB_\varphi = 0.01$ and $KnB_z = 0.005$.

$\gamma)/(1 + \gamma) > 0$ (near the periphery). As mentioned in Section 2, this means that at small wavelengths the observed polarization is either transverse $\Psi_{\text{obs}} = 0$ ($\gamma < 1$) or longitudinal $\Psi_{\text{obs}} = \pi/2$ ($\gamma > 1$) due to the jet symmetric structure, see Appendix A. Since γ determines the relative strength of the longitudinal and azimuthal field components, the observed profiles of $\Pi(0)$ can also, as well as the Faraday rotation measure profiles, constrain the jet magnetic field structure. However, this problem is beyond the scope of this study and will be presented in the next paper.

5 DISCUSSION

It should be noted, that the ‘inverse (or anomalous) depolarization’ was considered earlier in the context of the multifrequency polarimetry of spiral galaxies (Sokoloff et al. 1998) and AGN jets with helical magnetic fields (Homan 2012). Ferrière, West & Jaffe (2021) studied the general case of the magnetic field with a helicity and confirmed the influence of the helical magnetic field on the Faraday rotation. In Homan (2012), the problem was investigated numerically by solving the full equations of the radiative transfer for a cylindrical jet with the magnetic field similar to the one described in Section 4. In our paper, we present the analytical treatment for a wider range of magnetic field models. Also Murphy, Cawthorne & Gabuzda (2013) applied analytical expressions of the transverse polarization profiles for the helical magnetic field from Laing (1981) to assessing the magnetic field pitch-angle and the viewing angle (both in the emitting plasma frame) for the parsec jet of Mrk 501, successfully recovering the spine-sheath structure. However, they have not considered the internal Faraday rotation and focused solely on the helical magnetic field influence on the polarization profiles at a single frequency.

In our models, we do not consider the relativistic bulk motion of the jet. AGN jets at parsec scales are thought to have a highly relativistic speeds (Lister et al. 2016, 2019, 2021; Weaver et al. 2022), while for kpc-scale jets the bulk motion is sub or mildly relativistic (Walker 1997; Wardle & Aaron 1997; Arshakian & Longair 2004; Mullin & Hardcastle 2009; Meyer et al. 2016, 2017). However, as discussed in Murphy et al. (2013), the relativistic bulk motion induces Doppler boosting and aberration, which do not change the polarization profiles, provided that the jet’s velocity is constant across its width. Thus, similar to Murphy et al. (2013) we effectively consider the emission and rotation in the rest frame of the moving plasma. Jets from the flux limited samples have viewing angles $\approx 1/\Gamma$ (Vermeulen & Cohen 1994; Lister et al. 2019). It implies that in the plasma frame they are viewed nearly ‘side-on’ (Gabuzda 2021). Another consequence of the relativistic bulk motion, as noted by Homan (2012), is that in the comoving frame the plasma sees radiation with larger, $\propto D/(1+z)$, where D – Doppler factor of the Faraday rotating plasma bulk motion, z – redshift of the source, than the observed wavelength due to the Doppler effect. This implies that the internal rotation is enhanced even if the rotating particles are not thermal, but mildly relativistic, e.g. from the low end of the power-law energy distribution.

We stress, that in our models the transverse gradients of RM trace the jet magnetic field itself, not the magnetized sheath around the jet (e.g. Broderick & McKinney 2010; Clausen-Brown et al. 2011; Zamaninasab et al. 2013). Actually, this does not contradict to the previous studies of the blazar jets. The typical RMs observed in parsec-scale jets are quite modest ($\approx 100 \text{ rad m}^{-2}$ in 8–15 GHz band with 80 per cent of the jets in the MOJAVE sample showing $\text{RM} \leq 400 \text{ rad m}^{-2}$, Taylor 1998, 2000; Zavala & Taylor 2001; Hovatta et al. 2012). Even the larger values of RM ($\approx 1000 \text{ rad m}^{-2}$) observed in some jets (e.g. between 12 and 43 GHz in Algaba 2013) are not accompanied with large enough rotation to exclude the internal case. Moreover, depolarization of some sources as well as the observed circular polarization do require the internal rotation (Homan et al. 2009; Hovatta et al. 2012; Kravchenko et al. 2017). It is interesting that Homan (2012) considers the inverse depolarization and the internal rotation in a jet with a helical magnetic field. Strictly speaking, inverse depolarization is not a unique signature of the internal rotation: it can also occur for a partially resolved foreground Faraday screens if two emitting regions within the beam have different intrinsic polarization directions and different values

of RM. However, as noted in Homan (2012), jet features displaying this effect are reasonably isolated from other jet features and almost all of them reside in a jet with a transverse RM gradient (Hovatta et al. 2012). This could imply that the helical magnetic field drives both effects. We note that some observations clearly indicate the contribution of the external Faraday rotation because of the large polarization angle rotation proportional to the wavelength squared or the variability of RM (Taylor 2000; Zavala & Taylor 2001; Kharb et al. 2009; Gómez et al. 2011; Kravchenko et al. 2017), although some smooth variability could not exclude the rotation by the jet plasma (O’Sullivan & Gabuzda 2009). Another simple way to differentiate the transverse gradient of RM driven by the jet magnetic field from that generated in the jet sheath is to consider RM values at the edges of the jet. In models considered in this paper they should be zero because of the zero path-length (Laing 1981). However, the finite resolution, noise and contribution from the external screen could distort this simple picture.

6 CONCLUSIONS

The main conclusions of the paper, which is our first look at the synchrotron emission depolarization in AGN jets, can be summarized in two points:

(1) The axial symmetry of the magnetic field leads to a linear dependence of the polarization position angle on the wavelength squared. The proportionality coefficient depends on the aiming distance and allows to estimate the radial profiles of helical magnetic field components. Solving this inverse problem in general case will be done in the forthcoming paper.

(2) The presence of both the toroidal and longitudinal components of the magnetic field could result in the degree of the polarization having its maximum value at $\lambda > 0$ – contrary to Burn’s relation. In other words, the dependence of the polarization degree on the wavelength squared is not just a sinc-function. We derived the relations for the polarization degree transverse profiles for several magnetic field models, generalizing earlier results to the case of the internal Faraday depolarization.

Finally, we note that all formulas obtained in this paper make the reasonable assumption that jets are axisymmetric. This implies the proportionality of the polarization position angle and the wavelength squared. It is also interesting that the dependence of the polarization on the aiming distance allows us to consider the inverse problem of reconstructing the magnetic field profiles across the jet. From the mathematical point of view, the inference of the magnetic field profile requires a monotonic relation between the coordinate along the ray and the Faraday depth as well as axisymmetry. Therefore, although the proposed method cannot be used to reconstruct an arbitrary magnetic field structure, with the assumption of the unidirectional azimuthal field component⁴ the solution of the inverse problem seems quite feasible. Moreover, in the next paper this inverse problem will be solved completely through the solution of the Volterra integral equation.

ACKNOWLEDGEMENTS

We thank the anonymous referee for helpful comments and suggestions that significantly improved the presentation of the results. We thank Naga Varun for careful reading the manuscript and valuable

⁴However, some models violate this assumption (e.g. Mahmud et al. 2013).

advices. We are grateful to Dr R. Beck (MPIfR, Bonn) for stimulating discussions and ideas.

DATA AVAILABILITY

There is no new data associated with the results presented in the paper. All the previously published data has the proper references.

REFERENCES

- Albaga J. C., 2013, *MNRAS*, 429, 3551
 Anderson C. S., Gaensler B. M., Feain I. J., 2016, *ApJ*, 825, 59
 Arshakian T. G., Longair M. S., 2004, *MNRAS*, 351, 727
 Asada K., Inoue M., Uchida Y., Kameno S., Fujisawa K., Iguchi S., Mutoh M., 2002, *PASJ*, 54, L39
 Beskin V. S., Kniazev F. A., Chatterjee K., 2023, *MNRAS*, 524, 4012
 Blandford R., Meier D., Readhead A., 2019, *ARA&A*, 57, 467
 Brentjens M. A., de Bruyn A. G., 2005, *A&A*, 441, 1217
 Broderick A. E., McKinney J. C., 2010, *ApJ*, 725, 750
 Burn B., 1966, *MNRAS*, 133, 67
 Chen Y. J., Zhao G. Y., Shen Z. Q., 2011, *MNRAS*, 416, L109
 Christodoulou D. M., Gabuzda D. C., Knuettel S., Contopoulos I., Kazanas D., Coughlan C. P., 2016, *A&A*, 591, A61
 Cioffi D. F., Jones T. W., 1980, *AJ*, 85, 368
 Clausen-Brown E., Lyutikov M., Kharb P., 2011, *MNRAS*, 415, 2081
 Farnsworth D., Rudnick L., Brown S., 2011, *AJ*, 141, 191
 Ferrière K., West J. L., Jaffe T. R., 2021, *MNRAS*, 507, 4968
 Gabuzda D., 2017, *Galaxies*, 5, 11
 Gabuzda D., 2018a, *Galaxies*, 7, 5
 Gabuzda D. C., 2018b, *Proc. Int. Astron. Union*, 14, 189
 Gabuzda D. C., 2021, *Galaxies*, 9, 58
 Gabuzda D. C., Knuettel S., Bonafede A., 2015, *A&A*, 583, A96
 Gabuzda D. C., Roche N., Kirwan A., Knuettel S., Nagle M., Houston C., 2017, *MNRAS*, 472, 1792
 Gabuzda D. C., Nagle M., Roche N., 2018, *A&A*, 612, A67
 Ginzburg V. L., Syrovatskii S. I., 1966, *Phys. Usp.*, 8, 674
 Gómez J. L., Roca-Sogorb M., Agudo I., Marscher A. P., Jorstad S. G., 2011, *ApJ*, 733, 11
 Homan D. C., 2012, *ApJ*, 747, L24
 Homan D. C., Lister M. L., Aller H. D., Aller M. F., Wardle J. F. C., 2009, *ApJ*, 696, 328
 Hovatta T., Lister M. L., Aller M. F., Aller H. D., Homan D. C., Kovalev Y. Y., Pushkarev A. B., Savolainen T., 2012, *AJ*, 144, 105
 Jones T. W., O'Dell S. L., 1977, *ApJ*, 214, 522
 Kharb P., Gabuzda D. C., O'Dea C. P., Shastri P., Baum S. A., 2009, *ApJ*, 694, 1485
 Knuettel S., Gabuzda D., O'Sullivan S. P., 2017, *Galaxies*, 5, 61
 Komissarov S. S., Barkov M. V., Vlahakis N., Königl A., 2007, *MNRAS*, 380, 51
 Kravchenko E. V., Kovalev Y. Y., Sokolovsky K. V., 2017, *MNRAS*, 467, 83
 Laing R. A., 1981, *ApJ*, 248, 87
 Lisakov M. M., Kravchenko E. V., Pushkarev A. B., Kovalev Y. Y., Savolainen T. K., Lister M. L., 2021, *ApJ*, 910, 35
 Lister M. L. et al., 2016, *AJ*, 152, 12
 Lister M. L. et al., 2019, *ApJ*, 874, 43
 Lister M. L., Homan D. C., Kellermann K. I., Kovalev Y. Y., Pushkarev A. B., Ros E., Savolainen T., 2021, *ApJ*, 923, 30
 Lyutikov M., Pariev V. I., Gabuzda D. C., 2005, *MNRAS*, 360, 869
 Mahmud M., Gabuzda D. C., Bezrukova V., 2009, *MNRAS*, 400, 2
 Mahmud M., Coughlan C. P., Murphy E., Gabuzda D. C., Hallahan D. R., 2013, *MNRAS*, 431, 695
 Mantovani F., Mack K. H., Montenegro-Montes F. M., Rossetti A., Kraus A., 2009, *A&A*, 502, 61
 McKinney J. C., 2006, *MNRAS*, 368, 1561
 Meier D. L., Koide S., Uchida Y., 2001, *Science*, 291, 84
 Meyer E. T. et al., 2016, *ApJ*, 818, 195
 Meyer E. T. et al., 2017, *Galaxies*, 5, 8
 Motter J. C., Gabuzda D. C., 2016, *Galaxies*, 4, 18
 Mullin L. M., Hardcastle M. J., 2009, *MNRAS*, 398, 1989
 Murphy E., Cawthorne T. V., Gabuzda D. C., 2013, *MNRAS*, 430, 1504
 O'Sullivan S. P., Gabuzda D. C., 2009, *MNRAS*, 393, 429
 O'Sullivan S. P. et al., 2012, *MNRAS*, 421, 3300
 Park J., Hada K., Kino M., Nakamura M., Ro H., Trippe S., 2019, *ApJ*, 871, 257
 Pasetto A., 2021, *Galaxies*, 9, 56
 Pasetto A., Carrasco-González C., O'Sullivan S., Basu A., Bruni G., Kraus A., Curiel S., Mack K.-H., 2018, *A&A*, 613, A74
 Pasetto A. et al., 2021, *ApJ*, 923, L5
 Perley R. A., Bridle A. H., Willis A. G., 1984, *ApJS*, 54, 291
 Pushkarev A. B. et al., 2023, *MNRAS*, 520, 6053
 Rossetti A., Dallacasa D., Fanti C., Fanti R., Mack K. H., 2008, *A&A*, 487, 865
 Sokoloff D., Bykov A., Shukurov A., Berkhuijsen E., Beck R., Poezd A., 1998, *MNRAS*, 299, 189
 Taylor G. B., 1998, *ApJ*, 506, 637
 Taylor G. B., 2000, *ApJ*, 533, 95
 Tribble P. C., 1991, *MNRAS*, 250, 726
 Vermeulen R. C., Cohen M. H., 1994, *ApJ*, 430, 467
 Walker R. C., 1997, *ApJ*, 488, 675
 Wardle J. F. C., Aaron S. E., 1997, *MNRAS*, 286, 425
 Weaver Z. R. et al., 2022, *ApJS*, 260, 12
 Zamaninasab M., Savolainen T., Clausen-Brown E., Hovatta T., Lister M. L., Krichbaum T. P., Kovalev Y. Y., Pushkarev A. B., 2013, *MNRAS*, 436, 3341
 Zavala R. T., Taylor G. B., 2001, *ApJ*, 550, L147
 Zobnina D. I. et al., 2023, *MNRAS*, 523, 3615

APPENDIX A: PROPORTIONALITY OF POLARIZATION POSITION ANGLE TO THE WAVELENGTH SQUARED

Consider the polarization for the magnetic field structures symmetric about the Oxz -plane ($y = 0$), exactly such structures are used in this work and shown in three panels of Fig. 1. Rewrite the numerator I of the complex polarization ratio (2) using as integration variable the coordinate $y = r \sin \theta$ varying on the segment $[-l, l]$:

$$I = \int_{-l}^l \varepsilon(y) \exp(2i(\psi_0(y) + R(y)\lambda^2)) \left(\frac{dy}{\sin \theta} \right), \quad (\text{A1})$$

where all the functions included in the integral are expressed through the variable y . Assume that the emissivity function $\varepsilon(y)$ is even and reduce I to the integration over the segment $[0, l]$ by dividing the integral in the right side (A1) in two parts and substituting the variables $y \rightarrow -y$ in one of them. Thus, we obtain

$$I = \int_0^l \varepsilon(y) (\exp(2i(\psi_0(y) + R(y)\lambda^2)) + \exp(2i(\psi_0(-y) + R(-y)\lambda^2))) \left(\frac{dy}{\sin \theta} \right). \quad (\text{A2})$$

Rewrite the functions $R(y)$ and $R(-y)$ as

$$R(y) = Kn \int_{-l}^0 B_{\parallel}(y) \left(\frac{dy}{\sin \theta} \right) + Kn \int_0^y B_{\parallel}(y) \left(\frac{dy}{\sin \theta} \right), \quad (\text{A3})$$

$$\begin{aligned} R(-y) &= Kn \int_{-l}^{-y} B_{\parallel}(y) \left(\frac{dy}{\sin \theta} \right) = Kn \int_y^l B_{\parallel}(-y) \left(\frac{dy}{\sin \theta} \right) \\ &= Kn \int_0^l B_{\parallel}(-y) \left(\frac{dy}{\sin \theta} \right) - Kn \int_0^y B_{\parallel}(-y) \left(\frac{dy}{\sin \theta} \right), \end{aligned} \quad (\text{A4})$$

where $B_{\parallel}(y)dy$ is the magnetic field component parallel to the line of sight $-\mathbf{B}dr/|dr|$ expressed through y . For convenience introduce a substitution called the Faraday depth in Burn (1966):

$$\phi(y) = Kn \int_0^y B_{\parallel}(y) \left(\frac{dy}{\sin \theta} \right). \quad (\text{A5})$$

Assume that the function $B_{\parallel}(y)$ is even and the function $\psi_0(y)$ is odd. This assumption applies, for example, to the cylindrical regions considered in Fig. 1, if the angle $\psi_0(y)$ is zero on the x -axis. Rewrite the numerator I in (A2) as

$$I = \int_0^l 2\varepsilon(y) \cos(2\psi_0(y) + 2\phi(y)\lambda^2) \left(\frac{dy}{\sin \theta} \right) \exp(2i\phi(l)\lambda^2).$$

Substituting I in the ratio (2), we obtain formulas for the polarization angle Ψ and polarization degree Π . Moreover, for the angle we immediately obtain the proportional dependence $\Psi = \phi(l)\lambda^2$ with Faraday rotation measure equal $\text{RM} = \phi(l)$, and for the polarization degree, having done the same with the denominator of (2), we get

$$\Pi = \int_0^l \varepsilon(y) \cos(2\psi_0(y) + 2\phi(y)\lambda^2) dy \left| \int_0^l \varepsilon(y) dy \right|^{-1}. \quad (\text{A6})$$

Note once again that the direct proportionality $\Psi = \phi(l)\lambda^2$ is just a direct consequence of the parity of functions $\varepsilon(y)$ and $B_{\parallel}(y)$ and the oddity of function $\psi_0(y)$, i.e. their symmetry with respect to the Oxz-plane. For Burn's formula, there is also symmetry, see the left panel of Fig. 1. However, there is no oddness of the function $\psi_0(y)$: in the case of a constant field in the layer this function is equal to a constant. Thus, the dependence of the polarization angle on the wavelength squared becomes linear $\Psi = \psi_0 + \phi(l)\lambda^2$, while the polarization degree, on the contrary, does not include $\psi_0(y)$ and, after taking the integral, results in the famous sinc law (4).

APPENDIX B: TWO-ZONE MAGNETIC FIELD MODEL

Consider the model of a jet consisting of two parts: the central internal part, $0 \leq \rho \leq \rho_1$, with constant magnetic field $\mathbf{B} = (0, 0, -B_z)$ directed along the cylinder axis, and the periphery part, $\rho_1 \leq \rho \leq \rho_2$, with constant azimuthal magnetic field $\mathbf{B} = (B_\varphi \sin \varphi, -B_\varphi \cos \varphi, 0)$. The schematic representation of the areas are shown at the middle panel of Fig. 1. Suppose that the line of sight passes parallel to the Oyz-plane at the aiming distance x from the jet axis. If we introduce notations $l_1 = (\rho_1^2 - x^2)^{1/2}$ and $l_2 = (\rho_2^2 - x^2)^{1/2}$, then the peripheral region corresponds to the range $y \in [-l_2, -l_1] \cup [l_1, l_2]$, and the central region to the range $y \in [-l_1, l_1]$. Let's also assume that the change in the angle between the magnetic field \mathbf{B} and the line of sight dr from y coordinate can be neglected, so this angle φ is not defined by the equation $\cos \varphi = x/\rho$, but it is always equal to $\pm \varphi_0$, where $\cos \varphi_0 = x/\rho_2$. This implies that either the aiming distance is small or the periphery sheath is thin. In the first case, if the aiming distance x is small – for example, the ratio x/ρ_2 does not exceed 20 per cent – the angle φ is close to $\pi/2$ both here and there and the error in the angle does not exceed 15 per cent. In the second case, if the ratio $(\rho_2 - \rho_1)/\rho_2$ is small – for example, this ratio does not exceed 20 per cent – then the two cases are also close and the error between x/ρ_2 and x/ρ does not exceed 20 per cent, and accordingly the angles φ and φ_0 are close again. If both cases are true: x is small and $(\rho_2 - \rho_1)/\rho_2$ is small, then the accuracy of the used assumption is even greater and the error is even smaller.

The intrinsic polarization angle $\psi_0(r)$ is calculated as the angle between the northward direction $\mathbf{N} = (1, 0, 0)$ and the electric vector, estimated as the vector product of the magnetic field \mathbf{B} and the radiation direction vector $dr = (0, dy, dy \operatorname{ctg} \theta)$, thus its cosine can be

calculated as $\cos \psi_0 = \mathbf{N}(\mathbf{B} \times dr)/|\mathbf{B} \times dr|$. Therefore we obtain $\psi_0 = 0$ for the central area $y \in (-l_1, l_1)$ and

$$\cos \psi_0 = -x \cos \theta / \sqrt{\rho_2^2 - x^2 \sin^2 \theta} \quad (\text{B1})$$

for the peripheral area. In the degenerate case of $\theta = 90^\circ$ we get $\cos \psi_0 = 0$, but it is clear that since in the peripheral region the magnetic field vector \mathbf{B} has changed to the opposite one, than the vector $\mathbf{B} \times dr$ has changed to the opposite one, so we can consider that $\psi_0(y) = \pi/2$ for $y < 0$ and $\psi_0(y) = -\pi/2$ for $y > 0$. In other words, we can consider the intrinsic polarization angle ψ_0 as odd function with respect to $y = 0$. Note that the angle $\psi_0(y)$ itself is defined to within an additive constant $n\pi$, since it is in the argument of the exponent after the multiplier $2i$, see the formula (2). So at any point we can add π or remove it, i.e. change the sign of $\cos \psi_0(y)$ – mathematically it does not matter. This gives us a significant advantage when constructing an odd function from $\psi_0(y)$, see the Appendix A. We will not use it in our cases – because we get vector $\mathbf{B} \times dr$ with odd y and z components – but in other situations it may play a positive role.

Similarly, the emissivity $\varepsilon(y)$ is an even function. According to the assumption that it is proportional to the square of the field component transverse to the line of sight, we obtain ε_1 and ε_2 in the central and the peripheral areas correspondingly:

$$\varepsilon_1 = \kappa B_z^2 \sin^2 \theta \quad \text{and} \quad \varepsilon_2 = \kappa B_\varphi^2 (1 - x^2 \sin^2 \theta / \rho_2^2). \quad (\text{B2})$$

Let's calculate the auxiliary function $R(y)$ for three regions:

$$R(y) = Kn B_\varphi \cos \varphi_0 (l_2 + y), \quad y \in (-l_2, -l_1);$$

$$R(y) = Kn B_\varphi \cos \varphi_0 (l_2 - l_1) + Kn B_z \operatorname{ctg} \theta (y + l_1), \quad y \in (-l_1, l_1);$$

$$R(y) = Kn B_\varphi \cos \varphi_0 (l_2 + y - 2l_1) + 2Kn B_z \operatorname{ctg} \theta l_1, \quad y \in (l_1, l_2);$$

and with its help by the formula (2) calculate the degree and angle of polarization, which after integration take the form

$$\begin{aligned} \Pi = & \frac{1}{1+\gamma} \frac{\sin(\mathcal{R}_1 \lambda^2)}{\mathcal{R}_1 \lambda^2} \\ & + \frac{\gamma}{1+\gamma} \frac{\sin(\mathcal{R}_2 \lambda^2)}{\mathcal{R}_2 \lambda^2} \cos((\mathcal{R}_2 + \mathcal{R}_1) \lambda^2 + 2\psi_0), \end{aligned}$$

$$\text{and } \Psi = (\mathcal{R}_2 + \mathcal{R}_1/2) \lambda^2, \quad (\text{B3})$$

where for convenience we use the notation for the relative emissivity

$$\gamma = \frac{\varepsilon_2(l_2 - l_1)}{\varepsilon_1 l_1} = \frac{B_\varphi^2 \rho_2^2 - x^2 \sin^2 \theta}{B_z^2 \rho_2^2 \sin^2 \theta} \frac{l_2 - l_1}{l_1} \quad (\text{B4})$$

and intrinsic Faraday measures:

$$\mathcal{R}_1 = 2Kn B_z \operatorname{ctg} \theta l_1 \quad \text{and} \quad \mathcal{R}_2 = Kn B_\varphi x(l_2 - l_1) / \rho_2. \quad (\text{B5})$$

Note, that in the case of the line of sight perpendicular to the jet $\theta = 90^\circ$ – hereinafter we call this case the degenerate case – we obtain $\mathcal{R}_1 = 0$, field B_z in the central region does not rotate the polarization plane, and the main role is played by the depolarization in the peripheral region $\mathcal{R}_2 \neq 0$. The Faraday rotation measure $\text{RM} = \mathcal{R}_2$ in this case grows with increasing aiming distance, and the polarisation modulus is the difference between the constant and the sinc:

$$\Pi = \frac{1}{1+\gamma} - \frac{\gamma}{1+\gamma} \frac{\sin(2\mathcal{R}_2 \lambda^2)}{2\mathcal{R}_2 \lambda^2}.$$

In other words at short wavelengths the radiation is partially depolarized $\Pi(0) = |1 - \gamma|/|1 + \gamma|$, just as it is at longer wavelengths, where $\Pi(\infty) = 1/|1 + \gamma|$. The measures of these depolarizations are determined by the relative intensity γ of the magnetic fields, which in turn depends on the distance from the aiming distance x .

Another special case is that of a non-perpendicular line of sight, but directed exactly at the jet centre $x = 0$. In this case, $\mathcal{R}_2 = 0$ and the depolarization process is determined by the field in the central region rather than in the peripheral region. In this case, the Faraday rotation measure exactly coincides with the analogous value for a flat galaxy $\text{RM} = \mathcal{R}_1/2$, but the degree of polarization at $x = 0$ is equal to the difference

$$\Pi = \frac{1}{1 + \gamma} \frac{\sin(\mathcal{R}_1 \lambda^2)}{\mathcal{R}_1 \lambda^2} - \frac{\gamma}{1 + \gamma} \cos(\mathcal{R}_1 \lambda^2). \quad (\text{B6})$$

Again we have that at short wavelengths the radiation is partially depolarized $\Pi(0) = |1 - \gamma|/|1 + \gamma|$, just as it is at longer wavelengths $\Pi(\infty)$ oscillates with amplitude $\gamma/|1 + \gamma|$. The two considered cases are undoubtedly specific, in the general case the degree of polarization decreases at longer wavelengths. But the reduced polarization degree compared to the case of a flat galaxy is a typical feature of the two-zone jet model.

APPENDIX C: HELICAL MAGNETIC FIELD MODEL

Finally, let us consider a one-zone cylindrical model of a jet, $\rho < \rho_2$, with a helical magnetic field $\mathbf{B} = (B_\varphi \sin \varphi, -B_\varphi \cos \varphi, -B_z)$. We use the standard coordinate system shown in right panel of Fig. 1, and the standard line of sight passing at the aiming distance x from the jet axis. The angle $\varphi(y)$ in contrast to the two-zone jet model continuously depends on the y coordinate and is defined by $\cos \varphi = x/(x^2 + y^2)^{1/2}$ and $\sin \varphi = y/(x^2 + y^2)^{1/2}$, where $y \in [-l_2, l_2]$ and $l_2 = (\rho_2^2 - x^2)^{1/2}$. The intrinsic polarization angle $\psi_0(y)$ is calculated as the angle between the northward direction $\mathbf{N} = (1, 0, 0)$ and the vector $\mathbf{B} \times d\mathbf{r}$ just as in the Appendix B:

$$\cos \psi_0(y) = \frac{B_z \sin \theta - B_\varphi \cos \varphi \cos \theta}{\left((B_z \sin \theta - B_\varphi \cos \varphi \cos \theta)^2 + B_\varphi^2 \sin^2 \varphi \right)^{1/2}}.$$

It is important that $\psi_0(y)$ is again the odd function, since the y and z components of the vector $\mathbf{B} \times d\mathbf{r}$ are odd functions with respect to $y = 0$. According to the calculations in the Appendix A, it is straightforward to obtain the Faraday rotation measure for the helical field:

$$\begin{aligned} \frac{\Psi}{\lambda^2} &= \phi(l_2) = K n \int_0^{l_2} (B_\varphi \cos \varphi \sin \theta + B_z \cos \theta) \frac{dy}{\sin \theta} \\ &= K n B_\varphi x \ln |(\rho_2 + l_2)/x| + K n B_z \operatorname{ctg} \theta l_2 = \mathcal{R}_2 + \mathcal{R}_1/2, \end{aligned} \quad (\text{C1})$$

here $B_\varphi = \text{const}$ and $B_z = \text{const}$, and the intrinsic measures defined through these fields as $\mathcal{R}_1 = 2 K n B_z \operatorname{ctg} \theta l_2$ and $\mathcal{R}_2 = K n B_\varphi x \ln |(\rho_2 + l_2)/x|$. The first measure \mathcal{R}_1 that depends on the longitudinal field component has the form exactly the same as for the flat galaxy or for the two-zone model, except for the width of the active region l_2 . The second measure \mathcal{R}_2 is similar to that obtained for two-zone model, see Appendix B, but has a slightly different appearance. This is not surprising since the helical model takes into account the rotation of the azimuthal field B_φ along the line of sight.

Note that, in the general case, both measures \mathcal{R}_1 and \mathcal{R}_2 depend on the profiles of the azimuthal and longitudinal components of the magnetic field in the jet. The above formulas are calculated for a constant magnetic field, but they can be similarly calculated for the increasing, e.g. $B_\varphi(\rho) = B_\varphi \rho / \rho_2$, or decreasing, e.g. $B_\varphi(\rho) = B_\varphi \rho_2 / \rho$, fields correspondingly:

$$\mathcal{R}_2 = K n B_\varphi x l_2 / \rho_2 \quad \text{or} \quad \mathcal{R}_2 = K n B_\varphi \rho_2 \operatorname{arctg}(l_2/x). \quad (\text{C2})$$

In our opinion, it is not so much the specific form of each of the obtained distributions is fundamental here, but the explicit dependence of the Faraday rotation measure on the profiles of the longitudinal magnetic field B_z – responsible for the x -symmetric part of RM, and of the azimuthal magnetic field B_φ – responsible for the x -antisymmetric part of RM. These two dependences allow us to constrain the inverse problem of reconstruction of the magnetic field component profiles from the dependence of the Faraday rotation measure on the aiming distance x .

Similarly using the results obtained in (A6), we can rewrite the polarization degree for the helical model as equal to

$$\Pi(\lambda^2) = \frac{\int_0^{l_2} ((b_1^2 - b_2^2) \cos(2\phi\lambda^2) - 2b_1 b_2 \sin(2\phi\lambda^2)) dy}{\int_0^{l_2} (b_1^2 + b_2^2) dy} \quad (\text{C3})$$

with the emissivity $\varepsilon(y)$ proportional to the square of the perpendicular component of the magnetic field:

$$\begin{aligned} \varepsilon(y) &= \kappa (b_1^2(y) + b_2^2(y)) \quad \text{where} \quad b_2(y) = B_\varphi \sin \varphi \\ \text{and} \quad b_1(y) &= B_z \sin \theta - B_\varphi \cos \varphi \cos \theta. \end{aligned} \quad (\text{C4})$$

It is clear that, similar to the two-zone jet model, the observed radiation is partially depolarized at short wavelengths:

$$\Pi(0) = \left| \frac{1 - \gamma}{1 + \gamma} \right|, \quad \text{where} \quad \gamma = \int_0^{l_2} b_2^2(y) dy \left| \int_0^{l_2} b_1^2(y) dy \right|^{-1}. \quad (\text{C5})$$

For any given magnetic field component profile, it is possible to calculate γ and estimate this polarization drop, e.g. for the constant magnetic field $B_\varphi = \text{const}$ and $B_z = \text{const}$ we get γ equal to

$$\frac{B_\varphi^2(l_2 - x \operatorname{arctg}(l_2/x))}{B_z^2 \sin^2 \theta l_2 - x B_z B_\varphi \sin 2\theta \ln |(\rho_2 + l_2)/x| + x B_\varphi^2 \cos^2 \theta \operatorname{arctg}(l_2/x)}.$$

or for the magnetic field increasing with distance from the jet's centre $B_\varphi(\rho) = B_\varphi \rho / \rho_2$ and $B_z = \text{const}$ we obtain

$$\gamma = \frac{l_2^2 B_\varphi^2}{3\rho_2^2 (B_z \sin \theta - x B_\varphi \cos \theta / \rho_2)^2}. \quad (\text{C6})$$

But what is interesting here is not the particular value of γ , but the fact of polarization depression itself.

Using the obtained formula (A6), the degree of polarization Π can also be calculated. Of course, it will depend on the profile of the magnetic field, and in the simplest form of increasing to the jet edges field $B_\varphi(\rho) = B_\varphi \rho / \rho_2$ and $B_z = \text{const}$, when the Faraday depth ϕ and y coordinate are proportional, the degree of polarization will have the following form:

$$\Pi = \frac{1}{1 + \gamma} \left(1 + \sqrt{3\gamma} \frac{\partial}{\partial \xi} \right)^2 \frac{\sin \xi}{\xi}, \quad \text{where} \quad \xi = \mathcal{R}\lambda^2, \quad (\text{C7})$$

the intrinsic Faraday measure, see the first formula in (C2):

$$\text{RM} = \mathcal{R}/2 = \mathcal{R}_2 + \mathcal{R}_1/2 = K n B_\varphi x l_2 / \rho_2 + K n B_z \operatorname{ctg} \theta l_2, \quad (\text{C8})$$

and γ are defined by (C6). For the considered case, the polarization degree is a combination of sines and cosines – similar to the two-zone model. However, in our opinion, the most interesting is not the special form of the polarization degree for a particular case, but the fundamental possibility of setting the inverse problem of restoring the structure of the magnetic field by the observed polarization.

This paper has been typeset from a TeX/LaTeX file prepared by the author.